Photon assisted transport in superlattices beyond the nearest-neighbor approximation

Xian-Geng Zhao
Institute of Applied Physics and Computational Mathematics, P.O. Box 8009, Beijing 100088, China;
Department of Physics, University of Texas at Austin, Austin, Texas 78712;
and Institute of Theoretical Physics, Academia Sinica, P.O. Box 2735, Beijing 100080, China

G. A. Georgakis and Qian Niu
Department of Physics, University of Texas at Austin, Austin, Texas 78712
(Received 28 February 1997)

Transport properties in superlattices are studied at and beyond the nearest-neighbor approximation. Fractional resonant structures are found in the photon assisted transport characteristics when the second- and third-neighbor couplings are included. We have designed superlattice parameters for which such couplings are important. [S0163-1829(97)07131-2]

I. INTRODUCTION

Bloch electrons driven by a dc electric field show a variety of very interesting phenomena, including Bloch oscillations,[1] Wannier-Stark ladders,[2] and Landau-Zener tunneling.[3] These have been observed in high-quality superlattices,[4,5] optical ring resonators,[6] and more recently on ultracold atoms in accelerating optical potentials.[7] With the addition of a strong ac field, a number of interesting effects have been predicted, including dynamical localization,[8] band collapse,[9] and fractional Wannier-Stark ladders.[10] The object of the present work is to investigate possible manifestations of the fractional ladders in the transport properties of Bloch electrons in dc and ac fields.

In the presence of a pure dc field E_0, the dc current from a Bloch band was calculated by Esaki and Tsu,[11] and found to follow nonlinear I-V characteristics, which are Ohmic for small fields and with a negative slope (negative differential conductivity) at large fields. In between these two regimes, the current is peaked at a particular value of the field where the period of Bloch oscillations $\hbar/(eE_0d)$ equals the scattering relaxation time τ, where e is the electron charge, d the lattice constant, and $\hbar$ the Planck constant. Some experimental indications of such negative differential conductivity were reported in Ref. 12.

In the presence of an additional ac field, $E_1\cos\omega t$, a series of resonant structures are found theoretically in the I-V characteristics,[13] each of which has a shape similar to the original Esaki-Tsu characteristics, but are shifted from the origin by an integer l multiple of the ac frequency times $ed/\hbar$. This corresponds to the physical picture of electron transport through the Wannier-Stark ladders accompanied by multiple-photon absorption or emission. The strength of the lth resonant structure is proportional to the square of the Bessel function $J_l(eE_1d/\omega)$, which vanishes when eE_1d/ω is a zero. The conditions of dynamical localization and band collapse correspond to the situation of eE_1d/ω being a zero of J_0. When this happens, the original Esaki-Tsu structure near zero dc field disappears, and the absolute conductivity becomes negative there. These predictions have recently been observed in transport measurements in a superlattice irradiated by a terahertz laser.[14,15]

Previous theories of transport properties of Bloch electrons in dc-ac fields were based on a model of a single band with sinusoidal energy dispersion, or equivalently a tight-binding model with nearest-neighbor couplings only. While this may be reasonable for commonly used superlattice parameters, it does not represent all the generic properties of a Bloch band with nonsinusoidal energy dispersions. In this paper, we go beyond the sinusoidal or nearest-neighbor approximation to calculate the I-V characteristics, the differential conductivity, and the characteristics of harmonic generation. Beside the integer photon resonances described above, additional resonances are found at places where the Bloch oscillation frequency matches with fractional multiples of the photon frequency.

To give a practical example of our system, we will design an explicit superlattice structure in which the second- and third-nearest-neighbor couplings are important. In addition to a general analysis through analytical formulas (Sec. II), we also show some numerical results to give more concrete guide to possible future experiments (Sec. III). Finally, we will give some concluding remarks in Sec. IV.

II. GENERAL FORMULATION

We will calculate the transport properties in a regime where the particles remain within a single band, but we will take a general energy dispersion of the band under consideration,

$$\epsilon(k)=\sum_{n=0}^{\infty} R_n\cos(nkd), \tag{2.1}$$

where d is the superlattice period and R_n are the Fourier coefficients of the energy dispersion. In Sec. III, we will devise a realistic example where the terms beyond $n=1$, i.e., beyond nearest-neighbor hopping, are important.

In the absence of dissipation, the dynamics of the Bloch electrons is much like the periodically driven Josepheson junction.[16] Finite dc current can be generated if the Bloch oscillation frequency matches with an integer or fractional

multiple of the ac frequency, where the fractional multiples occur only when the energy dispersion is nonsinusoidal. When the device is put in a circuit in series with an ordinary resistor and a battery, the actual I-V characteristics of the device should consist of steps at voltages precisely equal to integer or fractional multiples of $\hbar\omega/e$. However, dissipation within the superlattice changes the picture quite substantially.

Our calculation is based on the Boltzmann equation in the relaxation-time approximation:

$$\frac{\partial}{\partial t} f(k,t) - eE(t) \frac{\partial}{\partial k} f(k,t) = -[f(k,t) - f_0(k)]/\tau. \tag{2.2}$$

Here $f(k,t)$ is the distribution function, $eE(t)$ a time-dependent electric force, τ the transport relaxation time, and $f_0(k)$ the Fermi-Dirac distribution function. From now on, we take the convention of $\hbar = 1$. The solution of this equation can be expressed as

$$f(k,t) = \int_{-\infty}^{t} \frac{dt'}{\tau} e^{-(t-t')/\tau} f_0\left(k + e\int_{t'}^{t} dt'' E(t'') \right), \tag{2.3}$$

where we have neglected the transient terms. The time-dependent current can be calculated from the formula $j(t) = -e\int v(k) f(k,t) dk$, where $v(k) = \partial\epsilon/\partial k$ is the velocity. Taking the dc-ac electric field $E(t) = E_0 + E_1\cos(\omega t)$, and assuming a low-temperature and low-density limit where the electrons are concentrated near momentum $k = 0$, we obtain the electric current as

$$j(t) = j_0 \sum_{n=1}^{\infty} n \frac{R_n}{R_1} \int_0^{\infty} \frac{ds}{\tau} e^{-s/\tau} \sin n \times \left(\omega_B s + \frac{edE_1}{\omega} (\sin\omega t - \sin\omega(t-s)) \right), \tag{2.4}$$

where $j_0 = eR_1$, and $\omega_B = edE_0$ is the frequency of Bloch oscillations. After expanding the integrand in terms of Bessel functions, the integral can be evaluated to yield

$$j(t) = j_0 \sum_{n=1}^{\infty} n \frac{R_n}{R_1} \sum_l J_l(nedE_1/\omega) \times \mathrm{Im}\left\{ \frac{e^{i((nedE_1/\omega)\sin\omega t - l\omega t)}}{1 - in\omega_B\tau - il\omega\tau} \right\}. \tag{2.5}$$

In the quasistatic situation, $\omega\tau \ll 1$, the above formula for the long-time current reduces to the following form:

$$j(t) = j_0 \sum_{n=1}^{\infty} n \frac{R_n}{R_1} \frac{n\tilde{\omega}_B(t)\tau}{(n\tilde{\omega}_B(t)\tau)^2 + 1}, \tag{2.6}$$

where $\tilde{\omega}_B(t) = ed(E_0 + E_1\cos\omega t)$. This formula can also be easily derived from Eq. (2.4) by expanding $\sin\omega(t-s)$ about $s = 0$. This formula states that the current is an instantaneous function of the total field, and the functional dependence is the same as that for the static situation, Eq. (2.7) below. In Ref. 17, the quasistatic formula was used to extract the ac components of the various harmonics, and plotted them as functions of the dc field. These agree with the experimental results well in overall shape, but do not reproduce some of the fine structures. In the following, we will work in the regime of $\omega\tau > 1$, where fine structures of resonances appear.

DC transport

In the absence of the ac field, the long-time current has only the dc component, given by

$$j_0 \sum_{n=1}^{\infty} n \frac{R_n}{R_1} \frac{n\omega_B\tau}{(n\omega_B\tau)^2 + 1}. \tag{2.7}$$

The $n = 1$ term is the well-known Esaki-Tsu I-V characteristics[11] $j = j_0\omega_B\tau/[(\omega_B\tau)^2 + 1]$, which arises linearly with the electric field E_0, peaked at $E_0 = 1/ed\tau$, and dies off at large field strength, yielding a negative differential conductivity. This phenomenon was observed experimentally,[12] which was regarded by some as an indication of the existence of Wannier-Stark ladders.[2] In general, the nth term contribution to the current is peaked at $E_0 = 1/ned\tau$, which can give rise to a shift of the Esaki-Tsu peak away from the result of the nearest-neighbor hopping approximation. Assuming that the main effect of the shift comes from the $n = 2$ term, then the shift is towards a larger value of the field if R_2/R_1 is negative, and toward a smaller value if R_2/R_1 is positive. In the example given in Sec. III, the former situation is realized.

Photon assisted transport

We first consider the simpler situation of nearest-neighbor approximation, where the dc current in the presence of the ac field is given from Eq. (2.5) by

$$j = j_0 \sum_{l=-\infty}^{+\infty} J_l^2(edE_1/\omega) \frac{\omega\tau(\omega_B/\omega - l)}{(\omega\tau)^2(\omega_B/\omega - l)^2 + 1}. \tag{2.8}$$

Under the condition $\omega\tau > 1$, peaks can appear at field values shifted from the Esaki-Tsu peak by an integer multiples of ω/ed, some evidence of which was seen in a recent experiment with the inverse Bloch oscillator effect.[15] The above result also shows that a peak corresponding to an integer l can be eliminated if the ac field strength makes the Bessel function $J_l(edE_1/\omega)$ nearly zero. In particular, the original Esaki-Tsu peak can be removed if $J_0(edE_1/\omega)$ is nearly zero.

We now look at the general situation beyond the nearest-neighbor approximation, and obtain the dc current from Eq. (2.5) as

$$j = \langle j(t) \rangle = j_0 \sum_{n=1}^{\infty} n \frac{R_n}{R_1} \times \sum_{l=-\infty}^{+\infty} J_l^2(nedE_1/\omega) \frac{\omega\tau(n\omega_B/\omega - l)}{(\omega\tau)^2(n\omega_B/\omega - l)^2 + 1}. \tag{2.9}$$

Additional peaks can appear at field values shifted from the Esaki-Tsu peak by fractional multiples of ω/ed. Such peaks are reflections of fractional Wannier-Stark ladders in the dc current.

Besides the dc current, one can also directly measure differential conductivity using the lock-in amplification technique, for which our formula becomes

$$\frac{dj}{d\omega_B}=\frac{j_0}{\omega}\sum_{n=1}^{\infty} n^2\frac{R_n}{R_1}\sum_{l=-\infty}^{+\infty} J_l^2(nedE_1/\omega) \times\frac{(1/\omega\tau)^2-(n\omega_B/\omega+l)^2}{(\omega\tau)[(1/\omega\tau)^2+(n\omega_B/\omega+l)^2]^2}. \quad (2.10)$$

The term for a given n and l is peaked at $E_0=(l/n)\times(\omega/ed)$, with a width $1/ned\tau$ which is increasingly narrower for larger n, and with a peak height given by $j_0n^2(R_n/R_1)\tau J_l^2(nedE_1/\omega)$ which may become negative for negative R_n/R_1 and oscillate with edE_1/ω. Also, because of the additional factor of n in the coefficient, the rich structures of the I-V characteristics can be more easily brought out in the differential conductivity.

Harmonic generation

We consider first the regime of $\omega\tau\gg1$, where only terms satisfying $n\omega_B+l\omega=0$ in (2.5) are important. The mth harmonic of the long-time current is given by

$$j_m=j_0{\sum_n}' n\frac{R_n}{R_1}J_{-n\omega_B/\omega}[J_{n\omega_B/\omega+m}-J_{n\omega_B/\omega-m}], \quad (2.11)$$

where the arguments of the Bessel functions are all $nedE_1/\omega$, and the symbol Σ_n' indicates a summation over those n satisfying $n\omega_B/\omega$ equal to an integer. In the absence of a dc field ($\omega_B=0$), the amplitude vanishes for even m, which is a result of time-reversal symmetry. The vanishing of even harmonics in the absence of a dc field is also obtained in the quasistatic limit for a different reason.[17] In general, such a result does not hold for finite $\omega\tau$ according to our formula (2.5), as is also evident from the experimental results of Ref. 17.

In the nearest-neighbor approximation, the above amplitude reduces to

$$j_m=j_0J_{-\omega_B/\omega}(edE_1/\omega)[J_{\omega_B/\omega+m}(edE_1/\omega) -J_{\omega_B/\omega-m}(edE_1/\omega)], \quad (2.12)$$

where ω_B must be an integer multiple of ω. For nonzero integers of ω_B/ω, the amplitude still vanishes when edE_1/ω is a zero of $J_{\omega_B/\omega}$, which is a result of band collapse. In general, in order to obtain a sizable amplitude of the mth harmonic, the ac field should have a strength with edE_1/ω comparable to or larger than the orders of the Bessel functions in the above equation. Such a condition can be made easier to satisfy if the dc field is chosen such that ω_B/ω is the integer part of $m/2$.

Beyond the nearest-neighbor approximation, the amplitude is nonzero even for fractional values of ω_B/ω. For example, if the fraction is p/q where p and q are mutually prime numbers, the leading term (in n) of the mth harmonic amplitude is given by

$$j_m=j_0q\frac{R_q}{R_1}J_{-p}(edE_1/\omega) \times[J_{p+m}(edE_1/\omega)-J_{p-m}(edE_1/\omega)]. \quad (2.13)$$

This is an oscillatory function of edE_1/ω, and vanishes when the latter is a zero of J_p, which is a manifestation of band collapse in the fractional Wannier-Stark ladders.

Therefore, when measured as a function of the dc field, the power of the mth harmonic ($\propto j_m^2$) shows a serious of peaks at integer values of ω_B/ω in the nearest-neighbor approximation, and with additional peaks at fractional values of ω_B/ω beyond the nearest-neighbor approximation. These peaks are broadened to a width of $\delta\omega_B=1/\tau$ when the scattering effect is taken into account. In the limit of $\omega\tau\ll1$, the peaks overlap and disappear into an overall envelope given by the quasistatic approximation (2.6).

III. NUMERICAL RESULTS

We consider a superlattice with GaAs wells of width a separated by $Al_xGa_{1-x}As$ barriers of thickness b. The conduction electrons can be well described by the Kronig-Penney model,[18] which leads to the eigenvalue equation for the energy dispersion $\epsilon(k)$ as

$$\frac{Q^2-K^2}{2QK}\sinh(Qb)\sin(Ka)+\cosh(Qb)\cos(Ka) =\cos[k(a+b)]. \quad (3.1)$$

Here $Q=\sqrt{2m(U-\epsilon)}$ and $K=\sqrt{2m\epsilon}$, where m is the effective mass of the electron, and U is the barrier height.

The barrier height U can be designed through the adjustment of the concentration x. For example, taking $x=0.3$, we have $U=0.3$ eV. We take in our model $a=40$ Å and $b=10$ Å, which leads to a superlattice period $d=50$ Å. Using these numbers and the effective mass $m=0.067m_e$ (m_e is the free-electron mass), from Eq. (3.1) for the first band we obtain $R_2/R_1=-0.202$ and $R_3/R_1=0.069$. The higher coefficients are very small, and will be ignored in the following calculations.

From the formulas derived in Sec. II we calculated the dc current j/j_0 and the differential current $(dj/d\omega_B)/(j_0/\omega)$ as functions of the dc bias ω_B/ω for different ac field strengths edE_1/ω. We took the scattering time to be $\tau=0.78T$, or equivalently $\omega\tau=4.9$, where T is the laser period $T=2\pi/\omega$. In the following, we display the results for three physical situations, and compare the results with and without the nearest neighbor approximation.

Figure 1 shows the dc current (upper panel) and the differential conductivity (lower panel) for the case of $E_1=0$, i.e., with the dc field only. The two curves for the dc currents have essentially the same shape, but the Esaki-Tsu peak for the lower curve is shifted slightly to the right due to the nonzero R_2. There is a similar rightwards shift of the structures for differential conductivity when couplings beyond the nearest neighbor are taken into account.

Figure 2 shows an example for $edE_1/\omega=0.9$, where the upper panel is still for the dc current, while the lower panel is for the differential conductivity. Besides the Esaki-Tsu peak of the dc current, a second peak appears near the position of

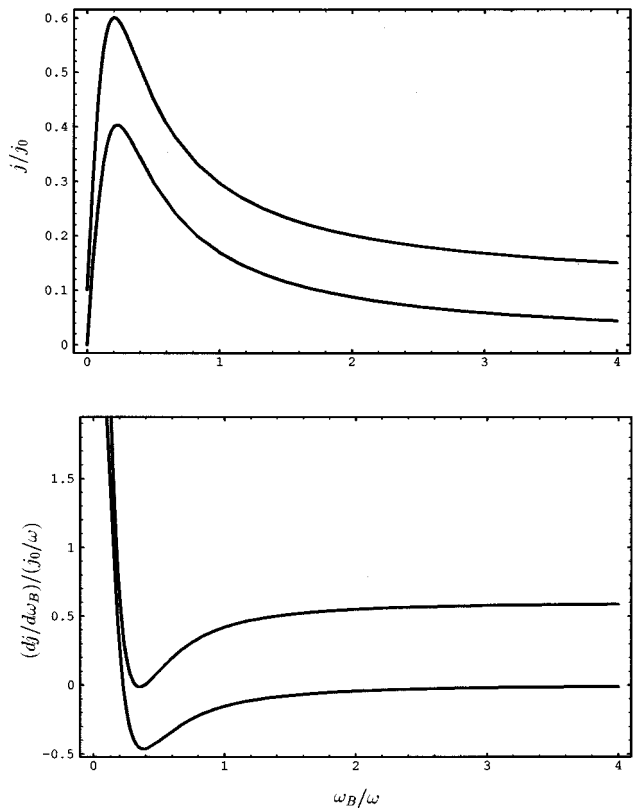

FIG. 1. The dc current (upper panel) and the differential conductivity (lower panel) of a superlattice under the action of pure dc fields. In both panels, the upper curve is for the case of the nearest-neighbor approximation, while the lower curve is for the case of long-range hoppings (up to third neighbor). We take $\omega\tau=4.9$. To avoid a crossing of the two curves, we shifted the upper curves upward by 0.1 in the upper panel, and 0.6 in the lower panel.

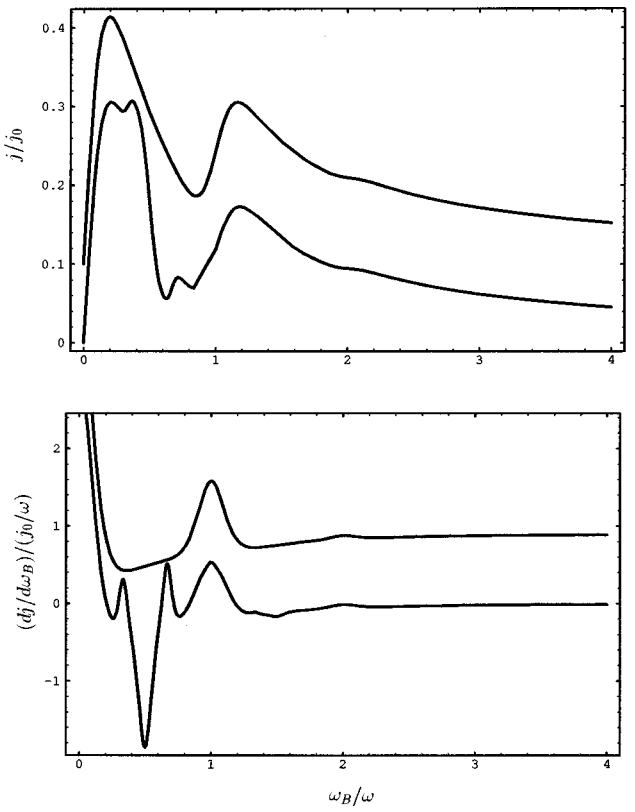

FIG. 2. The dc current (upper panel) and the differential conductivity (lower panel) of the superlattice under the influence of the ac field when $edE_1/\omega=0.9$. The upper and lower curves in both panels correspond to the cases of the nearest-neighbor approximation and beyond, respectively. We still take $\omega\tau=4.9$. The upper curves in the figure were shifted upward by 0.1 in the upper panel and 0.9 in the lower panel.

$\omega_B/\omega=1$ due to one-photon resonance, which was observed in a recent experiment.[15] Additional features emerge when we go beyond the nearest-neighbor approximation (lower curve). A small peak develops slightly to the right of the Esaki-Tsu peak, and another small peak develops near the valley between the Esaki-Tsu peak and the one-photon resonance.

A much clearer picture of the structures can be seen in the differential conductivity. The one-photon resonance now lies exactly at $\omega_B/\omega=1$. The fractional resonances in the lower curve (beyond the nearest-neighbor approximation) are shown as peaks at $\omega_B/\omega=\frac{1}{3}$ and $\frac{2}{3}$, and a deep valley at $\omega_B/\omega=\frac{1}{2}$. The reason for the structure at $\omega_B/\omega=\frac{1}{2}$ being a valley instead of a peak is that R_2 and R_1 have opposite signs. Degraded echoes of these structures also appear beyond the one photon resonance.

Figure 3 shows the case of $edE_1/\omega=2.405$. A remarkable result of this case is that the Esaki-Tsu peak in the dc current (upper panel) completely disappears, and correspondingly the differential conductivity (lower panel) becomes negative even at zero dc bias. This is a result of dynamic localization[8] because $edE_1/\omega=2.405$ is the first root of J_0, and this effect has now been observed in an experiment.[14]

Because of the larger ac field, multiple-photon resonances are much more pronounced than before. Also, the fractional resonances which occur beyond the nearest-neighbor approximation have much stronger echoes beyond the one-photon resonance. Here we remark that l-photon resonances can be quenched if edE_1/ω is a zero of J_l.

In Figs. 4–6, we show the behavior of the powers of harmonic generation as functions of ω_B/ω. In our plots, these powers are represented by the square of the ac current amplitudes, $|j_m|^2/j_0^2$, at the frequency of the ac field ($m=1$, Fig. 4) and its higher harmonics ($m=2$ and 3, Figs. 5 and 6). In each figure, the strength of the ac field is set, respectively, at $edE_1/\omega=1$ for the first column and at $edE_1/\omega=3.83$ for the second column. The upper panels are for the case of nearest-neighbor approximation, where we see peaks centered only at integer values of the horizontal axis, in agreement with the analytical formula (2.12). The power of the second harmonic vanishes at zero ω_B/ω, as is also expected from this formula. The finite width of the peaks are due to the finite relaxation time ($\omega\tau=4.9$). In the lower panels, we switch on the second- and third-neighbor couplings while keeping all the other parameters fixed. A comparison with the upper panels reveals some fractional structures.

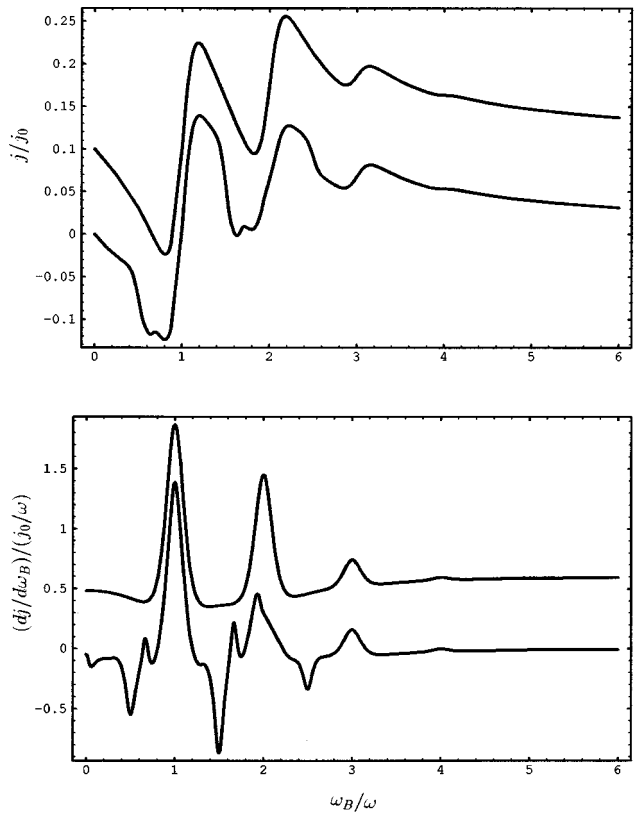

FIG. 3. The dc current (upper panel) and the differential conductivity (lower panel) of the superlattice under the influence of the ac field when $edE_1/\omega=2.405$, a zero of the Bessel function J_0. The upper and lower curves in both panels correspond to the cases of the nearest-neighbor approximation and beyond, respectively. We still take $\omega\tau=4.9$. The upper curves in the figure were shifted upward by 0.1 in the upper panel, and 0.6 in the lower panel.

IV. DISCUSSIONS

In summary, we studied the electronic transport properties in supperlattices at and beyond the nearest-neighbor approximation. We compared results for the pure dc transport, photon assisted transport, and harmonic generation. Fractional resonant structures are found in the case beyond the nearest-neighbor approximation, which are related to the fractional Wannier-Stark ladders proposed in our earlier publications.[10]

We have designed an explicit example of GaAs-$Al_xGa_{1-x}As$ superlattice in which the second- and third-neighbor couplings are important. A character of our model is that the barriers are narrower than those in commonly used superlattices. This makes the wave functions in the GaAs wells overlap strongly, and therefore results in wide minibands for the electronic spectrum. Consider a sample consisting of 80 periods of 40-Å-wide GaAs wells and 10-Å-thick $Al_{0.3}Ga_{0.7}As$ barriers, we have a width for the lowest miniband about 170 meV. The second miniband is separated from the first one by a gap about 110 meV. These two numbers are obviously comparable, but the fact does not contradict the single-band approximation used in our analysis as long as the bias is low enough (<400 mV).[19]

Under such low bias action, the Bloch frequency ω_B is in the THz range. Hence, to observe the fractional resonant structures, the laser frequency should be in the THz range. This is also the frequency range used in recent experiments on photon assisted transport.[20] Therefore, our theoretical

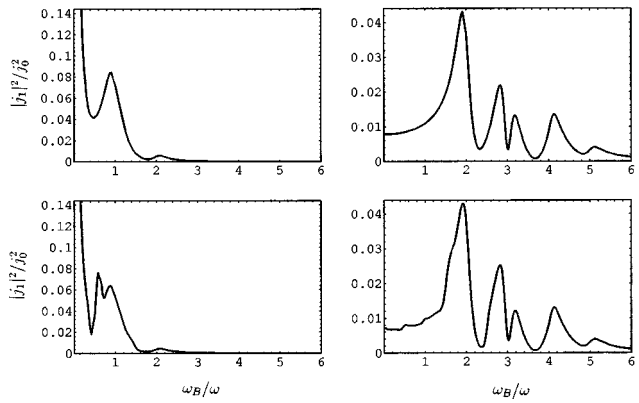

FIG. 4. Powers of the first-harmonic generation, $|j_1|^2/j_0^2$, as functions of ω_B/ω. The upper panels are for the nearest-neighbor approximation, while the lower panels are for the case with second- and third-neighbor couplings. In the left column, $edE_1/\omega=1$. In the right column, $edE_1/\omega=3.83$. In both cases, $\omega\tau=4.9$.

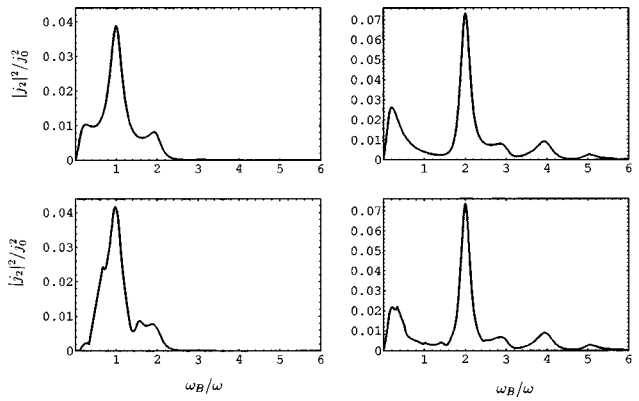

FIG. 5. Powers of the second-harmonic generation, $|j_2|^2/j_0^2$, as functions of ω_B/ω. The upper panels are for the nearest-neighbor approximation, while the lower panels are for the case with second- and third-neighbor couplings. In the left column, $edE_1/\omega=1$. In the right column, $edE_1/\omega=3.83$. In both cases, $\omega\tau=4.9$.

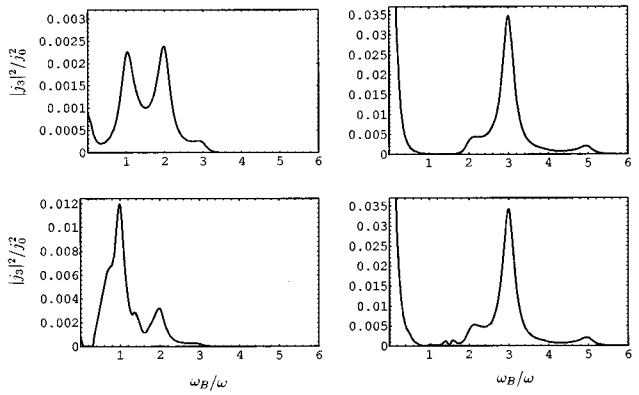

FIG. 6. Powers of the third-harmonic generation, $|j_3|^2/j_0^2$, as functions of ω_B/ω. The upper panels are for the nearest-neighbor approximation, while the lower panels are for the case with second- and third-neighbor couplings. In the left column, $edE_1/\omega=1$. In the right column, $edE_1/\omega=3.83$. In both cases, $\omega\tau=4.9$.

findings in this paper should be observable using the available experimental facilities.

ACKNOWLEDGMENTS

The authors are grateful to C. K. Ken Shih for the discussions on the experimental technique of differential conductivity measurement, and gratefully acknowledge the support of K. C. Wong Education Foundation, Hong Kong. The additional support was from the Robert A. Welch Foundation and the National Natural Science Foundation of China, and the grant of China Academy of Engineering and Physics.

[1] F. Bloch, Z. Phys. **52**, 555 (1929).

[2] G. H. Wannier, Phys. Rev. **117**, 432 (1960); Rev. Mod. Phys. **34**, 645 (1962).

[3] G. Zener, Proc. R. Soc. London, Ser. A **137**, 696 (1932).

[4] K. Leo, P. H. Bolivar, F. Brüggemann, R. Schwedler, and K. Köhler, Solid State Commun. **84**, 943 (1992); J. Feldmann, K. Leo, J. Shah, D. A. B. Miller, J. E. Cunningham, T. Meier, G. von Plessen, A. Schulze, P. Thomas, and S. Schmitt-Rink, Phys. Rev. B **46**, 7252 (1992); C. Waschke, H. G. Roskos, R. Schwedler, K. Leo, H. Kurz, and K. Köhler, Phys. Rev. Lett. **70**, 3319 (1993).

[5] E. E. Mendez and G. Bastard, Phys. Today **46** (6), 34 (1993).

[6] R. J. C. Spreeuw, N. J. van Druten, M. W. Beijersbergen, E. R. Eliel, and J. P. Woerdman, Phys. Rev. Lett. **65**, 2642 (1990).

[7] Q. Niu, X.-G. Zhao, G. A. Georgakis, and M. G. Raizen, Phys. Rev. Lett. **76**, 4504 (1996); M. Ben Dahan, E. Peik, J. Reichel, Y. Castin, and C. Solomon, *ibid.* **76**, 4508 (1996); S. R. Wilkinson, C. F. Bharucha, K. W. Madison, Q. Niu, and M. G. Raizen, *ibid.* **76**, 4512 (1996).

[8] D. H. Dunlap and V. M. Kenkre, Phys. Rev. B **34**, 3625 (1986); X.-G. Zhao, Phys. Lett. A **155**, 299 (1991); **167**, 291 (1992).

[9] M. Holthaus, Phys. Rev. Lett. **69**, 351 (1992).

[10] X.-G. Zhao and Q. Niu, Phys. Lett. A **191**, 181 (1994); X.-G. Zhao, R. Jahnke, and Q. Niu, *ibid.* **202**, 297 (1995).

[11] L. Esaki and R. Tsu, IBM J. Res. Dev. **14**, 61 (1970); R. Tsu and L. Esaki, Phys. Rev. B **43**, 5204 (1991).

[12] A. Sibille, J. F. Palmier, F. Mollot, H. Wang, and J. C. Esnault, Phys. Rev. B **39**, 6272 (1989); A. Sibille, J. F. Palmier, H. Wang, and F. Mollot, Phys. Rev. Lett. **64**, 52 (1990).

[13] V. V. Pavlovich and E. M. Epshtein, Fiz. Tekh Poluprovodn. **10**, 2001 (1976) [Sov. Phys. Semicond. **10**, 1196 (1976)].

[14] B. J. Keay, S. Zeuner, S. J. Allen, K. D. Maranowski, A. C. Gossard, U. Bhattacharya, and M. J. W. Rodwell, Phys. Rev. Lett. **75**, 4102 (1995).

[15] K. Unterrainer, B. J. Keay, M. C. Wanke, S. J. Allen, D. Leonard, G. Medeiros-Ribeiro, U. Bhattacharya, and M. J. W. Rodwell, Phys. Rev. Lett. **76**, 2973 (1996).

[16] A. A. Ignatov, K. F. Renk, and E. P. Dodin, Phys. Rev. Lett. **70**, 1996 (1993); A. A. Ignatov, E. Schomburg, J. Grenzer, K. F. Renk, and E. P. Dodin, Z. Phys. B **98**, 187 (1995); D. H. Dunlap, V. Kovanis, R. V. Duncan, and J. Simmons, Phys. Rev. B **48**, 7975 (1993).

[17] J. Grenzer *et al.*, Ann. Phys. (Leipzig) **4**, 265 (1995).

[18] C. Kittel, *Introduction to Solid State Physics*, 6th ed. (Wiley, New York, 1986), p. 165.

[19] A general argument can be found from A. Nenciu and G. Nenciu, Phys. Lett. A **78**, 101 (1980).

[20] H. Drexler, J. S. Scott, S. J. Allen, K. L. Campman, and A. C. Gossard, Appl. Phys. Lett. **67**, 2816 (1995).